Journal of The Electrochemical Society, **148** (11) A1239-A1246 (2001)
0013-4651/2001/148(11)/A1239/8/$7.00 © The Electrochemical Society, Inc.

In Situ Deposition and Ultrahigh Vacuum STM/AFM Study of V_2O_5/Li_3PO_4 Interface in a Rechargeable Lithium-Ion Battery

A. E. Semenov, I. N. Borodina, and S. H. Garofalini

Department of Ceramics and Materials Engineering, Rutgers-The State University, Piscataway, New Jersey 08854-8065, USA

A thin-film solid-state battery was prepared with a vanadium pentoxide cathode and a lithium phosphate electrolyte and studied *in situ* by ultrahigh vacuum scanning tunneling microscope/atomic force microscopy (STM/AFM). Orientation of the (001) plane of V_2O_5 parallel to the substrate was detected via observation of the periodicity of 11.7 ± 0.5 Å, which is consistent with the unit cell spacing in the ⟨100⟩ direction. Conductance of the battery was studied locally with the probe tip of the STM/AFM in the regime of mechanical contact with a constant repulsive force. Lateral variation of contact conductance from 0.4 to 2.2 nA was detected as a function of position of the tip in contact with the cathode. The device revealed an extremely high current density of 1 A/cm^2 due to the low thickness of the electrolyte and the cathode and the concentration of electric field under the scanning probe microscope tip. Transformation of cathode structure due to Li ion intercalation was observed in real time.
 [DOI: 10.1149/1.1406492]

Manuscript submitted January 23, 2001; revised manuscript received May 17, 2001. Available electronically September 28, 2001.

Thin-film solid-state microbatteries have been studied with great interest in recent years because of their potential applications in microelectronics, communications, smart cards, and medical devices.[1-4] Li-ion conducting devices have been the focus of this research because of their light weight and high energy density. Typically, a microbattery consists of a lithium-containing anode, a separating film of some lithium ion conducting electrolyte, and a cathode material capable of intercalation of the lithium into its own structure.[3] The entire film structure is usually coated with a final layer to serve as an electrical contact and protective layer. Much of the effort in the development of these batteries has focused on the properties of the individual films[3,5-9] and new materials are constantly being evaluated.[7,10-12]

Clearly, the performance of these devices must depend not only on the bulk properties of the individual film materials, but also on interface behavior. However, while there have been studies of the interface between liquid electrolytes and electrodes,[13] there have been far fewer studies of interfaces in solid-state devices because of the difficulty of accessing buried interfaces. There has been interest in the possibility of microheterogeneity in the conductance of a thin film device, but no direct analysis of such heterogeneity has been presented.

In the work presented in this paper, we have used *in situ* deposition and ultrahigh vacuum scanning probe microscopy (UHV-SPM), which includes UHV scanning tunneling microscopy (STM) and UHV atomic force microscopy (AFM) to address interface structure and heterogeneity in solid-state oxide Li-ion conducting thin-film devices. The electronic effects can be very local in STM due to the effect of the concentration of the electric field at the probe tip and the tunneling effect, allowing manipulation of a molecule[14,15] or ion,[16,17] including mechanical transfer and chemical reduction with electron injection. By placing the UHV-SPM probe tip in mechanical contact with the substrate battery, the tip can be used as an electrode of the battery to apply an electric potential at a specific place on the substrate and measure local conductance. By using the UHV-SPM in the scanning tunneling mode, surface topography with near atomic resolution is possible. This combination enables us to associate local conductance with local structure at the interface of the *in situ* deposited layers and address heterogeneity with nanometer resolution. In addition, transformation of the deposited cathode structure during charge and discharge of device can be studied via SPM in real time.

The thin-film cathode/electrolyte system investigated in this work is vanadium pentoxide (V_2O_5) interfaced with a lithium phosphate electrolyte glass. The anode side consists of a planar highly ordered pyrolytic graphite (HOPG) in contact with $LiCoO_2$ powder as the Li ion source. While this is clearly not an appropriate battery combination, it was used to study the local structure and electrical conductance of the V_2O_5 cathode at the early stages of cathode thin-film formation (20-30 nm thickness). The HOPG was used to create a flat surface upon which to deposit the thin layers of electrolyte and cathode. Vanadium pentoxide has the ability to incorporate alkali into its network because of its open planar structure (Fig. 1a); a thin- film lithium phosphate glass can be used as the electrolyte.[5,6] This cathode/electrolyte combination has been the used in solid-state batteries and electrochromic thin films; however,

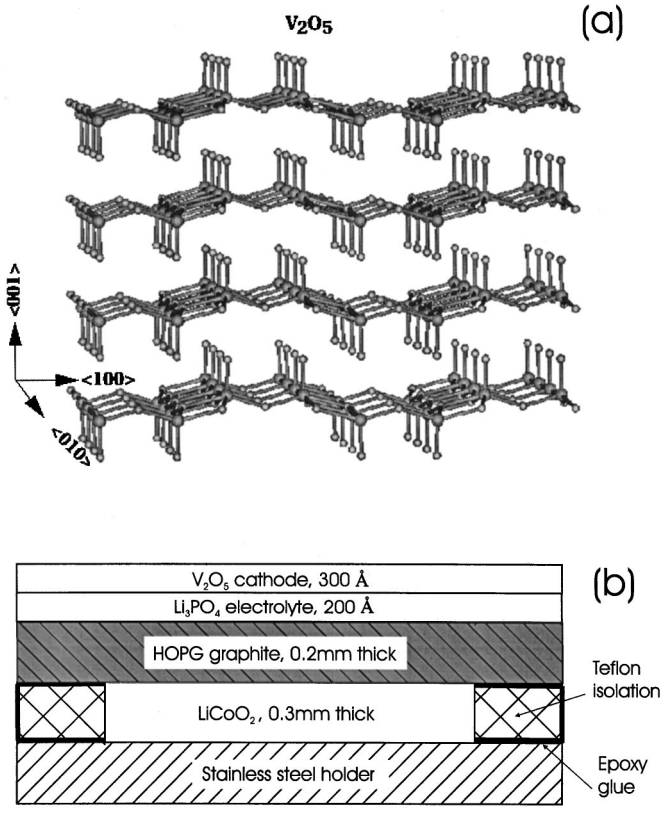

Figure 1. (a) Structure of V_2O_5. The larger spheres are vanadium and the smaller spheres are oxygen. (b) The diagram representing the multilayer structure of the experimental thin-film battery.

the intent of the work presented here is to study an appropriate model interface rather than study the newest (and ever changing) materials that are in vogue for thin-film batteries. In addition, the use of V_2O_5 as the cathode enables a potential correlation of the experimental results with our molecular simulations of interface behavior occurring between a Li-ion conducting glassy oxide electrolyte and V_2O_5.[18,19]

Experimental

The substrate consists of a thin-film solid electrolyte Li_3PO_4 glass and a thin film of the V_2O_5 cathode deposited *in situ* on an atomically flat surface of the anode (Fig. 1b). To create the atomically flat anode, HOPG was mounted by epoxy glue on the stainless steel holder with the $LiCoO_2$ powder between the HOPG and the stainless steel sample holder. The graphite was electrically isolated from the stainless steel holder by a strip of Teflon film on the edges of the holder and fixed with epoxy glue. HOPG with a lateral size of 8×8 mm and thickness of 0.2 mm has a contact area with the $LiCoO_2$ of 5×5 mm. The layer of $LiCoO_2$ powder was slightly pressed with pressure of 10^6 Pa to the final thickness of 0.3 mm. The graphite was cleaved with tape in the air before the *in situ* deposition of the electrolyte.

The film of lithium phosphate electrolyte glass was deposited by radio frequency (rf) magnetron sputtering using a 1 in. diam UHV/compatible Torus 1 magnetron sputter system from K. Lesker Co. (Clairton, PA). The lithium phosphate films were deposited using lithium phosphate targets made by pressing Li_3PO_4 powder. (Aldrich Chemical Co.) into disks at a pressure of 2×10^8 Pa, and sintering at 900°C for 2 h. Densities were observed to be 80% of theoretical. The target with a thickness of 3.8 mm was then ground down to the appropriate size in order to fit into the magnetron.

The rf sputter deposition was done in a two-stage UHV chamber with a base pressure of 10^{-9} Torr after baking. This system has been described previously.[20] While this background pressure was maintained in the SPM analysis side of the chamber, the deposition side was opened after bakeout in order to change sputter targets and insert new substrates. As a result, background pressures of 5×10^{-8} Torr were typical in deposition chamber. Sputter deposition was done using a 1 in. diam magnetron source from K. Lesker Co. The source was powered by an rf power supply and impedance matching circuit from Applied Energy. The source to sample distance was 10 cm. Thickness of the films were monitored by a quartz crystal deposition monitor (Leybold Inficon Inc.) located 3 cm from the sample. For deposition of lithium phosphate films, ultrahigh purity argon was used as the working gas and a pressure of 5 mTorr was maintained. The rf power was 50 W and rates of 4 Å per minute were observed. A lithium phosphate electrolyte film of 200 Å was deposited onto the HOPG. The substrate containing the $LiCoO_2$ below the HOPG below the thin-film glassy electrolyte was transferred to the UHV-SPM analysis chamber for characterization immediately after deposition of the electrolyte.

After UHV-SPM measurements of the electrolyte layer, the sample was transferred back to the deposition chamber. The vanadium pentoxide film was deposited by reactive sputtering of a 99.5% pure vanadium target obtained commercially (K. Lesker Co.) using a working gas with a composition of 16% O_2 and 84% Ar. The pressure was 16 mTorr and the power was 50 W. Thickness of the V_2O_5 cathode film was 300 Å as measured by a quartz crystal deposition monitor.

UHV-SPM (UHV-STM, UHV-AFM) was used to characterize the structural and electrical properties of the electrolyte and the cathode thin films. V, PtIr, and W probe tips were used at various stages of analysis.

Results

Conductance of the substrate device was monitored at all stages of preparation. Resistance between the stainless steel (SS) holder and the graphite through the layer of $LiCoO_2$ measured in air by digital multimeter immediately after preparation of the anode was 10^8 Ω. A current of 100 nA was detected at −10 V applied to the graphite. Subsequent *in situ* depositions of the electrolyte and cathode were done in the UHV-SPM and conductance analyses were done under UHV conditions.

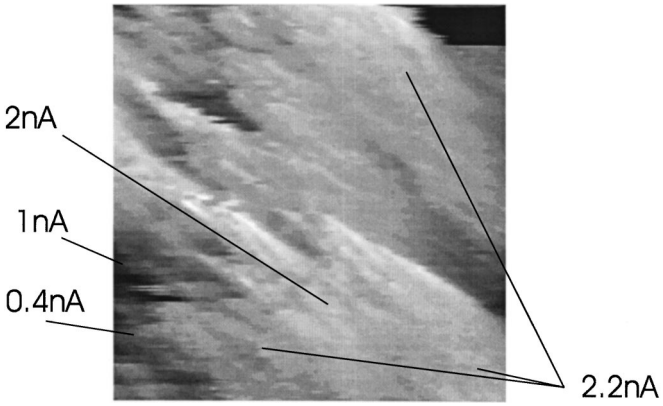

Figure 2. Distribution of current at the voltage of −1.8 V on the tip was obtained with the probe contacted to the surface of V_2O_5 mechanically at constant repulsive force in UHV. STM constant current image parameters are side of 530 Å, height range of 370 Å, $V_{tip} = -1.8$ V, $I = 250$ pA.

In situ deposition of the lithium phosphate electrolyte glass created a system of SS\$LiCoO_2$\graphite\electrolyte that showed typical resistance of 2×10^{10} Ω while the UHV-STM tip mechanically touched the surface.

Deposition of ~300 Å of vanadia over the electrolyte in the device reduced the resistance of the whole structure between the tip touching the surface of the vanadia and SS holder to 5×10^7 Ω due to higher conductivity of the cathode relative to conductivity of the electrolyte. If the tip touches the electrolyte, the diameter of current filament through the electrolyte is about the thickness of electrolyte, *i.e.*, ~200 Å. If the tip touches the cathode deposited over the electrolyte, diameter of current filament through the electrolyte is 3000 Å in our case. Measurements of this contact conductance performed with vanadium and PtIr probe tips cut in the air before experimental measurement showed no dependence of these electrical properties on the tip material.

In order to address the proposed heterogeneity of conductance of a thin-film battery and the effect of structure on that heterogeneity, UHV-STM and UHV-AFM analyses of local cathode structure, forces, and the associated contact conductance were performed. In these analyses, a W-probe tip was used. For STM images with near atomic resolution the W tip was cleaned *in situ* by heating with an electron beam to 900°C in UHV before usage. For combined AFM and STM analysis the W tip had not been heat cleaned, and therefore, had a native oxide film (WO_3) on its surface.[20] This latter tip had a soft cantilever elastic constant of 17 N/m.

The local conductance occurring in the cathode was studied using the UHV-SPM probe tip in mechanical contact (repulsive force) with feedback open. The results are shown in Fig. 2. The image itself was obtained in constant current UHV-STM mode. The contact current from 0.4 to 1.0 nA was detected in black areas of the image shown in Fig. 2 and from 2.0 to 2.2 nA in the white areas at the tip voltage of −1.8 V. The force was also monitored during this experiment. The force remained constant with an accuracy of 2.7×10^{-8} N and deflection of the cantilever was constant with an accuracy of 10 Å. While the conductance was not sensitive to such variations of force in the contact regime, it was sensitive to changes to lateral position. The results shown in the figure indicate a factor of 5 difference in the conductance from one local region to another, with a lateral separation distance of less than 200 Å. Thus, a local nanoheterogeneity in conductance is observed for the first time

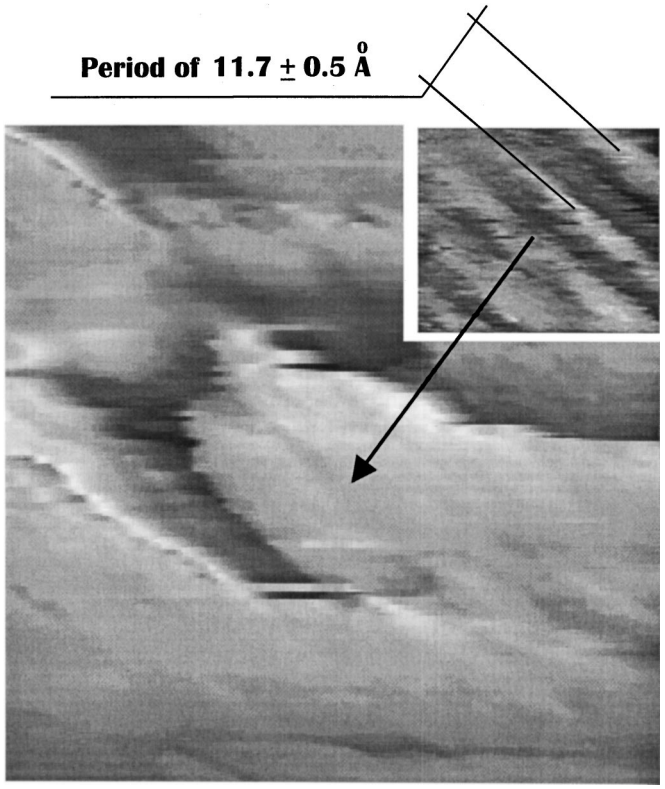

Figure 3. Periodical structure presented on the inset was observed in UHV at the bright area in the center of the large-scale image of V_2O_5. Side of inset of 53 × 45 Å. Height range of 130 Å, I = 90 pA, U_{tip} = −1.5 V. Side of large-scale STM constant current image of 1060 Å. Height range: 360 Å, I = 250 pA, V_{tip} = −1 V. Probe of W annealed at 900°C.

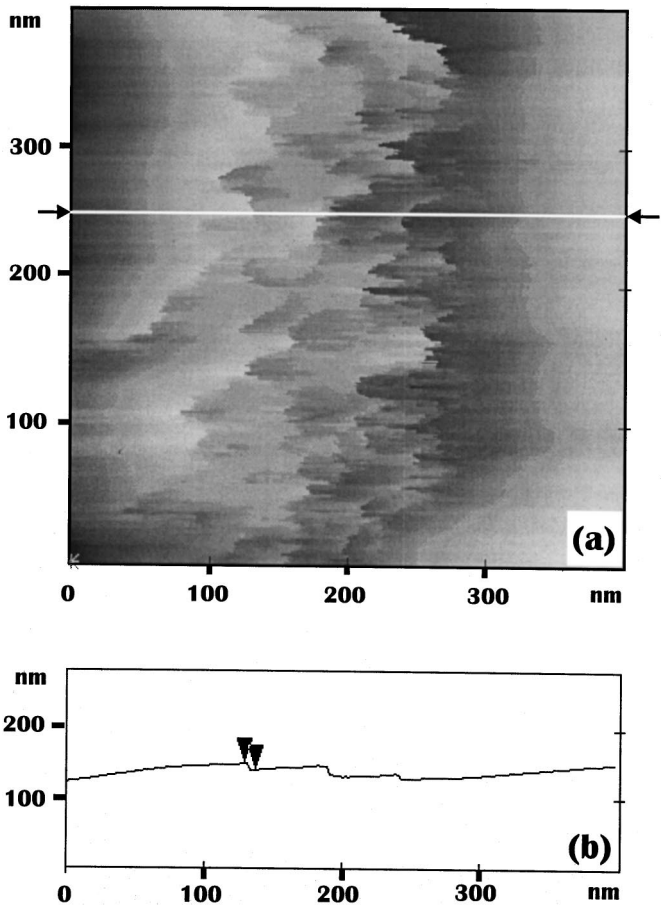

Figure 4. (a) AFM image of V_2O_5 surface taken at constant force in air. Height range of 100 nm. (b) Section along the line shown by arrows in Fig. 4a. Height of step between marks: 9 nm.

at the cathode/solid electrolyte interface. This heterogeneity in contact conductance is associated with the local structure of the cathode rather than the electrolyte.

Orientation of the deposited V_2O_5 crystal lattice was determined with UHV-STM. Figure 3 shows a large-scale constant current image with sides of 1060 Å. The bright areas indicate high topography while the dark areas indicate lower topography. In addition, as shown above with respect to Fig. 2, the bright areas are also associated with higher mechanical contact conductance.

The inset in Fig. 3 shows a periodic structure within an area of 53 × 45 Å located at the area near the center of the large-scale image. This periodic structure has a spacing of 11.7 ± 0.5 Å and corresponds to the V_2O_5 crystal having its (001) planes oriented parallel to the substrate. This spacing is consistent with the unit cell spacing in the **a** direction ($\langle 100 \rangle$), indicating the separation between the vanadyl pairs. This is shown schematically in Fig. 1. The two other possible orientations, with the (010) or (100) planes parallel to the interface, would each have a much smaller periodicity (~3.5 to 4.5 Å). However, the ~11.7 ± 0.5 Å periodicity seen here requires higher resolution to distinguish the crystal from being V_2O_5 doped with Li ions or a δ-Li V_2O_5 phase. It should be noted that additional images with similar periodicity were observed in other areas of the vanadia film. In addition to this periodic structure being observed in the bright area of the substrate, this structure was also detected in the flat gray areas. Crystallographic structure of the darkest areas was not resolved (Fig. 3 and 2).

While the crystal structure of a large single crystal of reduced V_2O_5 has been imaged via ambient STM,[21] Fig. 3 shows the first image of the crystal structure of an *in situ* deposited V_2O_5 thin film with unit cell (1 nm) resolution. In previous studies of solid oxide thin-film batteries using layered cathodes, X-ray diffraction data of <50 nm films indicated that the (003) planes were parallel to the cathode/electrolyte interface while thicker films indicated that the (003) planes were perpendicular to the interface.[7] The orientation of the V_2O_5 (001) planes parallel to the interface is consistent with studies of monolayer adsorption of V_2O_5 deposited onto silica substrates for catalyst studies.[22] Such results corroborate our scanning probe microscopy (SPM) data. In additional support for the orientation of the V_2O_5 films in our samples, we analyzed the battery studied here using a Nanoscope II in the constant force AFM mode. Results showed steps in the deposited films that were multiples of 0.44 nm spacing, consistent with the spacing in the $\langle 001 \rangle$ direction, again indicating that the (001) planes are parallel to the interface. Figure 4a presents an AFM image taken in the constant force mode in air. The quality of images was sufficiently high so as to enable measurement of the heights of the monatomic steps, as shown in Fig. 4b. The heights of 330 steps were measured and the statistics of small size steps up to a height of 4 nm are summarized in the histogram in Fig. 5.

Besides providing the first images of the crystal structure of an *in situ* deposited vanadia thin film at the initial stages of formation, the results imply that Li ion transport into the vanadia may have to occur perpendicular to the (001) planes. Of course, Li diffusion in the cathode could be more complicated based on the precise orientation or misorientation of the planes at the interface. Molecular simulations of Li ion transport into vanadia show a high activation barrier to migration across the (001) planes (in the $\langle 001 \rangle$ direction) as compared to migration between the planes (in the $\langle 010 \rangle$ or $\langle 100 \rangle$ directions).[18,19]

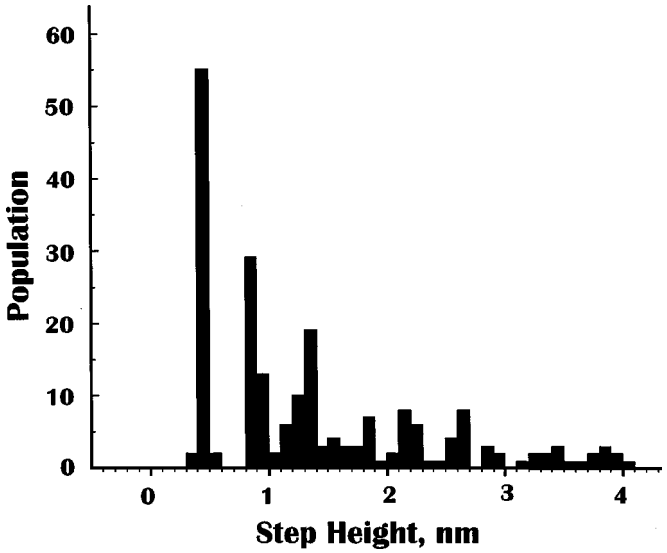

Figure 5. Histogram presents statistics of height of steps measured on V_2O_5 surface by AFM at constant force in air. Steps are multiples of 0.44 nm spacing, consistent with the spacing in the ⟨001⟩ direction.

Figure 6 shows a series of UHV-STM/AFM images of one area of the deposited cathode layer as a function of time at constant current and bias. Also shown in the Fig. 6g is a scan of the height *vs.* position along a line of zero force as established in the UHV-AFM mode. This force was measured concurrently during the constant current feedback.

Changes in the surface structure of V_2O_5 were observed after several frames of scanning with UHV-SPM at -2 V on the tip. Figure 6a-f presents a series of STM height and AFM force images taken on the same area at constant current mode with a time interval of 2 min between images. The white box within each image shows the same area, indicating the drift occurring in the SPM. Large flat terraces with lateral sizes of ~200 Å and thickness of 110 ± 22 Å are visible in Fig. 6a. The large terraces gradually transform during scanning into small terraces with lateral sizes of 36 ± 0.7 Å and heights of 46 ± 15 Å by Fig. 6e.

The variation in structure may be attributed to Li intercalation into the V_2O_5 caused by the voltage applied to the tip. The spacing between the (001) crystal planes of vanadia (see Fig. 1) is increased as Li ions intercalate (eventually to form the δ-Li_2O_5 phase), which also reduces bonding between the planes. This weakening between planes may enable sliding of the planes induced by the movement of the probe tip.

Using combined UHV-AFM and STM, force measurements were performed to distinguish between the contribution of geometrical relief and the variation of conductance and deformation on the topography obtained by UHV-STM.

Figure 6g presents the height variation along the zero force line shown in the Fig. 6a. The force between the tip and sample is almost constant and zero along this line, causing minimal deformation of the sample. Based on this analysis, the real amplitude of relief variation was estimated to be 60 Å. The amplitude of relief variation taken in a constant force mode in the AFM image shown in Fig. 4 is 90 Å.

Figures 6a and b show the constant current STM topography and force image, respectively, taken at the same place on the surface. Force imaging was done using the signal from the laser interferometer force sensor while feedback was monitored by STM. Both images reveal an in-phase variation of contrast. The force image was not sensitive to the scanning rate, so force contrast is not due to noncoordination of feedback. A plot of force (F) *vs.* current (I) presented in Fig. 7 could explain the origin of contrast in the force image. Figure 7 indicates a negative derivative (dF/dI) at voltage of -2 V and the current of 140 pA used in the STM and force imaging. The gap between the tip and the surface is smaller at the low conductive spots at constant current, force lower (more attractive) and dark spots appear in-phase in both topography and force image.

The bright spots of topography reveal repulsive forces in Fig. 6b after the first frame of the series of images, and zero force at the last frame in Fig. 6f. The plot F *vs.* I current in Fig. 7 shows similar behavior. A repulsive force at a current of 140 pA was detected at engagement of the tip. Force is shifted toward attraction at withdrawal of the tip. The repulsive force observed in Fig. 7 could be attributed to a long range electrostatic interaction.

The time dependent measurement of the local current was performed with the STM probe tip in contact with the cathode of the battery. The voltage of $+4$ V was applied to the oxidized W tip in mechanical contact with the surface for 5 min, after which the voltage on the tip was switched to $V_{tip} = -4$ V. The time dependence of current after the voltage was switched was measured as shown in Fig. 8. This figure demonstrates that near saturation of current occurs within ~1 s, followed by a very slow increase in current. The conductance of the battery after completion of this process is about two times higher than in the beginning. We ascribe this process to local doping of the cathode with Li^+ ions that enhances the electrical conductivity of the cathode, as discussed below.

Of course, the migration of Li ions through the electrolyte into cathode requires the injection of electrons into cathode from an external circuit. A typical voltage-current characteristic (volt-amp characteristic, VAC) taken during mechanical contact between the PtIr tip and vanadia is presented on Fig. 9. Results identical to those shown in Fig. 9 were obtained using a V tip and a PtIr tip cut in air. The VAC is shown to provide evidence of the conductive behavior of the cathode film. The exponential behavior of the current may be explained as involving (a) activated Li ion diffusion into the cathode, (b) electron transfer from the tip via a Poole-Frenkel bulk electron emission mechanism or by a Schottky emission at the electrode,[23] or a combination of a and b. The Poole-Frenkel bulk mechanism and Schottky emission at the electrode can be described by

$$I = AT^2 \exp(\beta_S V^{1/2} - \phi_0)/k_B T \quad \text{(Schottky emission)} \quad [1]$$

$$I = B \exp(\beta_{PF} V^{1/2} - \phi_1)/k_B T \quad \text{(Poole-Frenkel emission)} \quad [2]$$

where $\beta_{PF} = \beta_S = 2(e^3/4\pi\varepsilon\varepsilon_0 d)^{1/2}$ where e is the electronic charge, d is the thickness of the thickness of the film, k_B is the Boltzmann constant, ε_0 is the dielectric constant of free space, and ε is the relative dielectric constant of the material of the film. The VAC shows the expected exponential behavior that indicates the presence of some barriers between the tip and the cathode or within the cathode film. The voltage-current characteristic in Fig. 9 shows that there is no dielectric breakdown at any voltage below the 8 V shown.

Figure 10 shows several VAC curves of charging this device at near zero voltages. The battery was charged with different voltages applied to the tip of -0.1, -1, -2, -3, -4, and -5 V for 1 min before the VAC was taken. The voltage was switched from the "setup" voltage to the sweeping voltage within 10 μs. The sweeping voltage was 2.5 V/s. The feedback was open and the tip was in mechanical contact with the vanadium oxide surface. There is a finite current at zero external voltage in the same direction as would occur with a negative bias on the tip, indicating no back-current of electron through the external circuit in the opposite direction. This finite current increased at zero voltage with increasing setup voltage. Such a model battery was charged to 50 mV between cathode and stainless steel electrode by external voltage $V_{tip} = -5$ V. Figure 11 presents an equivalent scheme of the battery and STM in our experiments. The input resistance of the preamplifier was 2 MΩ. The sum of capacitance of the battery and the preamplifier was less

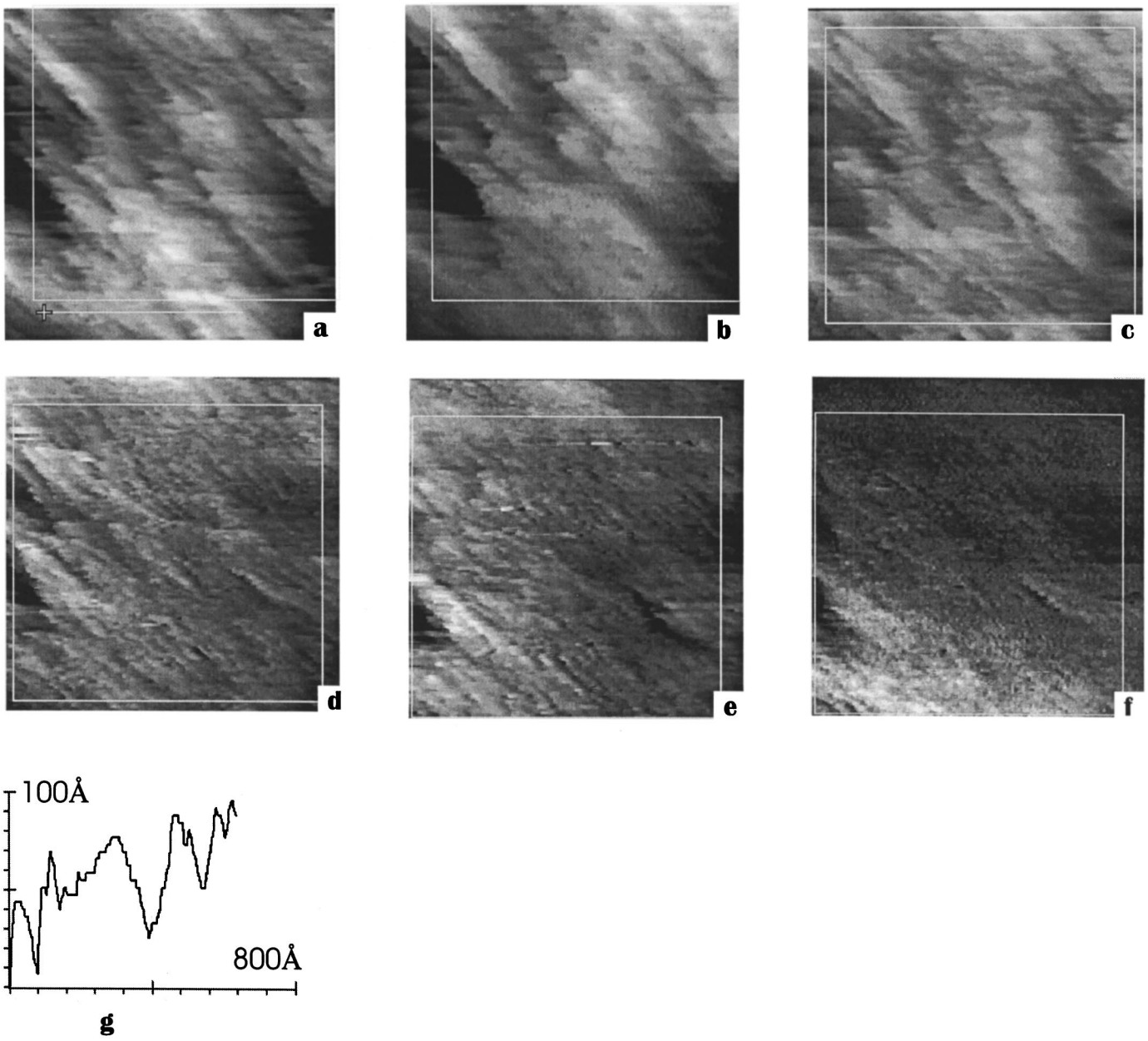

Figure 6. Series of STM and AFM images of vanadia with side of 1060 Å were taken in UHV on the same are with interval of 2 min at constant current $I = 140$ pA and $V_{tip} = -2$ V. (a) (c) (d) and (e) are STM height images; height range: 340 Å. (b) Force image, force range from -5×10^{-7} to $+5 \times 10^{-7}$ N. (f) Force image, force range from -5.6×10^{-7} N to zero. (g) Section along the line with zero force shown in a. Result of intercalation of vanadia with Li ions is visible. Large slabs with lateral size of 200 Å and thickness of 110 ± 22 Å gradually transform into small terraces with lateral size of 36 ± 0.7 Å and height of 46 ± 15 Å.

than 22 pF measured by a Wavetek 28XT multimeter and this capacitance was omitted on the equivalent scheme. The internal resistance of the battery was of 2.7 MΩ in this experiment. The low observed voltage of the battery was due to the very similar electrochemical potential of Co^{3+} and V^{5+}. Both battery 1 formed by interface $LiCoO_2$-graphite and battery 2 with the structure graphite-electrolyte-V_2O_5, presented in Fig. 11, have opposite signs and a near equal value of voltage. For comparison, the voltage of a Li-V_2O_5 cell in experiment 6 was 3.6 V and the voltage of a Li-$LiCoO_2$ cell was of 4.2 V [24] with an electrolyte of lithium phosphorus oxynitride in both experiments.

The low voltage of our experiment battery of ~50 mV helps distinguish between spatial variation of electrochemical potential and variation of conductance of vanadia by STM imaging. Voltage of the battery is much smaller than the voltage of the external circuit, so variation of the current due to variation of electrochemical potential could be only 5% and is negligible compared to the spatial variation of current by the factor of 5.5 observed in Fig. 6.

Behavior of VAC presented in Fig. 10 provides evidence for the chemical nature of the source of voltage on the battery due to lithium migration. With zero external voltage the current flows in the same direction as at the previously applied negative voltage on the tip. It means Li ions move still in the same direction to V_2O_5. There was no hysteresis in the voltage-current characteristics (*i.e.*, VAC was not influenced by charge of capacitance on the input of the preamplifier and the capacitance of the battery).

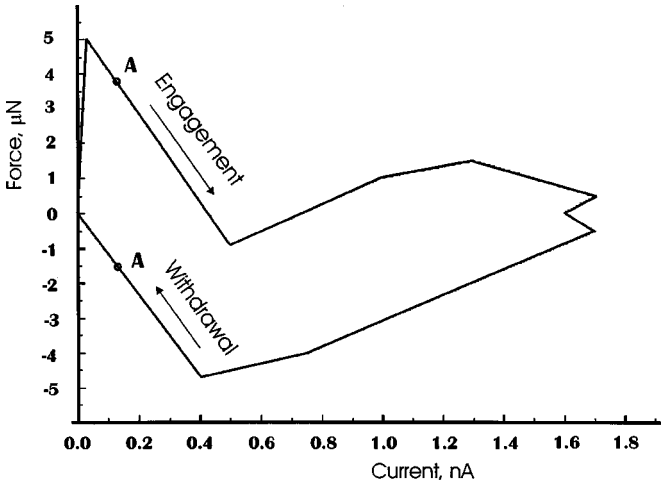

Figure 7. Plot force *F vs.* current *I* at feedback off reveals negative derivative dF/dI at voltage $V_{tip} = -2$ V and current $I = 140$ pA used by STM and force imaging in Fig. 2. Letter A in the plot marks that point. Repulsive force at current of 140 pA was detected at engagement of the tip. Force is shifted toward attraction at withdrawal of the tip.

Discussion

The conductivity of the layers measured at every step of battery preparation enabled calculation of the current distribution through the cathode and the electrolyte for our configuration of electrodes. Conductance is attributed to a combination of electron injection into the cathode at the tip/cathode interface as well as Li ion migration into the cathode at the electrolyte/cathode interface.

The tip is under a negative potential, so an excess of electrons injected into the surface of vanadia from the tip could reduce vanadium from V^{+5} to V^{+4} and induce repulsion of the tip, as seen with respect to Fig. 6b and f, and Fig. 7. Negative charge at the surface dissipates with time after scanning due to migration of Li^+ ions through the electrolyte toward the surface of V_2O_5. As a result, a repulsive force does not appear in the final Fig. 6f. Low conductive dark areas reveal permanent attractive force in Fig. 6b and f due to lower mobility of charge.

The area of current filament through the battery in our STM experiment was estimated to be $\sim 10^{-9}$ cm^2 immediately upon engagement of the tip. While this is the current filament through the battery due to the electric field normal to the interface, there is also a gradient of Li concentration in the V_2O_5 perpendicular to that filament (parallel to the vanadia layers). This gradient allows for lateral migration of Li in each layer of V_2O_5 until full saturation of the film volume occurs. As shown in Fig. 8, the conductance of the cathode increases with time; however, the lateral migration of Li due to the concentration gradient also increases the area of the current filament through the battery. Hence, in Fig. 8, the rapid increase in the current within ~ 1 s after the change of polarity is ascribed to growth of the local specific conductivity of V_2O_5 at the contact area near the tip due to migration of Li^+ along the electric field normal to the surface. The subsequent slower growth of current is due to the increasing of the area of the current filament by lateral migration of Li^+ along the Li concentration gradient.

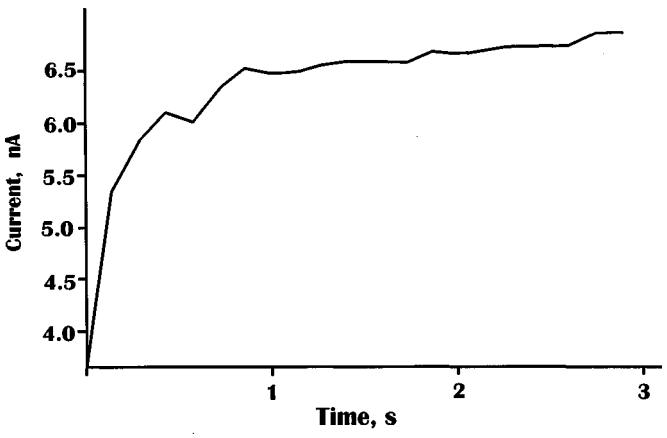

Figure 8. Local current demonstrates saturation with character time of the process of 1 s after voltage on the tip was switched from +4 to −4 V. The STM probe tip touched the cathode.

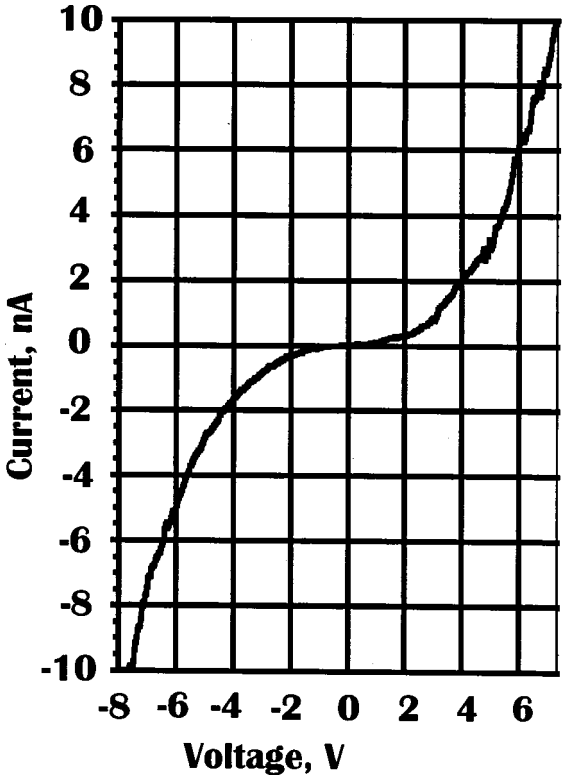

Figure 9. Typical voltage-current characteristic taken at a mechanical contact between the PtIr tip and vanadia.

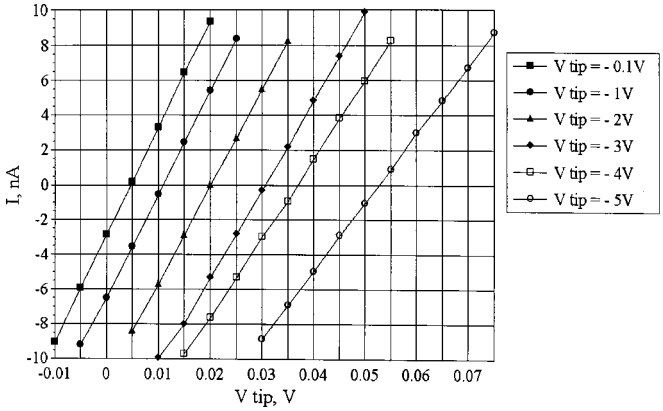

Figure 10. VAC near-zero voltages. Battery was charged with the tip voltage of −0.1, −1, −2, −3, −4, and −5 V for 1 min. Battery demonstrates nonzero current at zero external voltage and zero current at positive voltage on the tip. Battery loaded by STM preamplifier shows voltage of 50 mV after charging with voltage of −5 V.

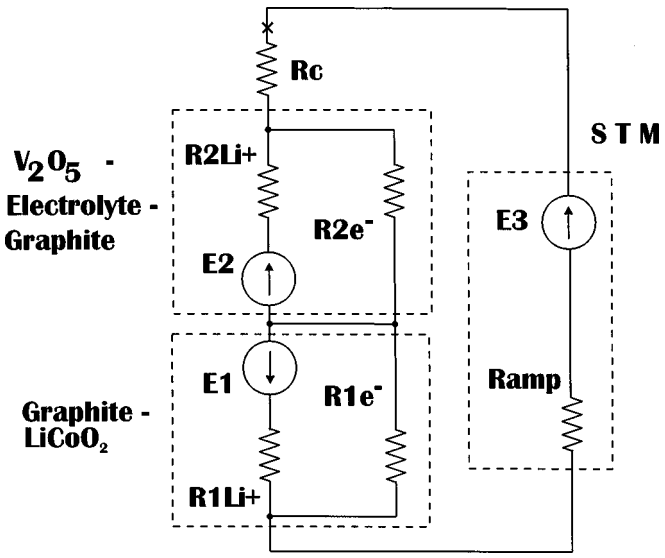

Figure 11. Equivalent scheme of model battery in STM experiment. Two opposite electromotive forces $E1$ and $E2$ are partially shunted through electronic resistance ($R1e^-$, $R2e^-$) and ionic resistance ($R1Li+$, $R2Li+$) of interface $LiCoO_2$-graphite and electrolyte, respectively. Film cathode with resistance Rc is in contact with the tip of STM closing the circuit by input resistance of preamplifier ramp and source of voltage E3.

With the tip of SPM in contact with the surface of the thin cathode layer, an extremely high current density of ~1 A/cm^2 with 60% voltage drop on internal resistance occurred in this study. A current density of 0.1 mA/cm^2 was reached in Bates' work[6] for a thin film battery using a V_2O_5 cathode without excessive voltage drop due to internal resistance. The cathode and electrolyte films were each of about 1 μm thick in that work.[6] Current densities of 10 mA/cm^2 were observed by the same group on the plane cells with $LiCoO_2$ cathodes with a loss of 70% of their maximum capacity.[24] We explain the higher current density in our experiment as being caused by two effects: (*i*) lower thickness of electrolyte and cathode and (*ii*) the concentration of the electric field directly under the tip. Lower thickness creates a 25 times higher electric field in the electrolyte and the cathode compared to the previous work.[6,24] An additional factor of 4 excess of current in our experiment compared to the previous work[24] could be explained by the electric field concentration at the tip.

Previous molecular dynamics computer simulations indicated the formation of a Li-rich layer at the cathode/electrolyte interface[19] and was similarly suggested in experimental work done by Bae *et al.*[25] The simulations give an activation energy of ~2.5 eV for Li ion diffusion perpendicular to the V_2O_5 (001) planes, which is much higher than the value of Li ion diffusion in the electrolyte glass (~8 eV).[19] This causes a difficulty of Li ion migration in the cathode with the (001) planes parallel to the interface, causing an accumulation of Li at the interface. In experimental work, Bae *et al.*[25] find a similar accumulation of Li and discuss an associated decrease in electrode potential caused by the filling and accumulation of Li ions in the cathode/electrolyte interface. They also detected a decrease in diffusivity which was assigned to the increased Li-Li interaction and a decrease of available sites in the crystal.

The device studied with the SPM behaves differently because of the presence of the SPM tip and the associated electric field. The SPM tip creates a distribution of field with a higher field on the outer side of the cathode near the tip and a lower field at the cathode/electrolyte interface.[26] This higher density of field lines near the tip in comparison to the cathode/electrolyte interface creates an increased field (force) on the Li ions toward the tip, effectively lowering the barriers caused by the (001) orientation of the vanadia planes. The activation barrier in each layer closer to the tip is lowered in comparison to those closer to the electrolyte, enabling faster transport of Li to the tip side of the cathode. This concurrently depletes layers nearer the electrolyte side of the cathode of Li, thus removing the additional barrier to migration caused by Li-Li repulsions and site competition, enabling faster transport of Li into the cathode. Concentration of the electric field at the tip produces the trap with a low potential for Li ions on the tip side of the cathode. Thus the low thickness of cathode, combined with the localization caused by the SPM tip, provides an electric field high enough to enable a high rate of diffusion and to prevent accumulation of Li at the cathode/electrolyte interface. In this case, we suppose Li ions accumulate in the tip side of cathode first and then Li ions fill layers down to the cathode/electrolyte interface layer by layer. Molecular dynamics simulations showed that the activation energy for Li ion diffusion between the planes, in the ⟨010⟩ direction is, much lower (~8 to 9 eV) than that for diffusion across the layers in the ⟨001⟩ direction mentioned above.[19] The simulations support a spread of the Li ions within the planes.

The effect of the tip and the associated concentrated electric field and the lowering of the activation barriers for Li ion diffusion into the cathode as Li ions approach the tip is different from what would occur with a uniform current collector in contact with the cathode, or from what is seen in the simulations which do not use a localized field.

The influence of any possible inhomogeneous conductivity of Li in the electrolyte could not be determined in our SPM experiments. This is due to the lower electrical resistance of the V_2O_5 in our experiment compared to the resistance of the electrolyte, plus the fact that the current in our experiment is collected at the STM tip from an area of the cathode and the electrolyte with a lateral diameter of ~3000 Å.

Possible local shortages with electronic conductivity in the electrolyte do not influence the neighboring areas in our STM experiment. Every area studied with the probe is practically independent of other parts of the battery. This is an important advantage of STM that enables the study of very thin layers of electrolyte and cathode. Significant statistics can be easily taken by changing the probe position on the sample.

Conclusion

Orientation of V_2O_5 lattice was locally determined with UHV-STM. The observed periodicity of 11.7 ± 0.5 Å corresponds to the (001) plane of V_2O_5 oriented parallel to the substrate. Additional analysis that showed steps on the vanadia planes equal to ~0.44 nm, consistent with the lattice spacing in the ⟨001⟩ direction, corroborated the interpretation of the orientation of the deposited polycrystalline film. Transformation of cathode structure due to Li ion intercalation was also observed.

Conductivity of the battery was studied locally with the probe tip of UHV-STM/AFM in the regime of mechanical contact with a constant repulsive force. The variation in current was detected from 0.4 to 2.2 nA in nearby areas of the UHV-STM image. The battery formed with the SPM probe in contact with the surface of the thin layer cathode revealed an extremely high current density of 1 A/cm^2. Two effects may explain this high current density, (*i*) the low thickness of electrolyte and cathode and (*ii*) the concentration of the electric field under the tip of SPM. Experiments with different thickness of cathode are in progress.

Acknowledgments

We would like to acknowledge support from the U.S. DOE Division of Chemical Sciences, grant no. DE-FG02-93ER14385. Also, the authors thank E. Koray Akdogan for help preparing the target for deposition of the electrolyte, and Alvin J. Salkind for useful discussions.

Rutgers-The State University assisted in meeting the publication costs of this article.

References

1. See, for example, B. V. R. Chowdari and S. Radhakrishna, Editors, in *Solid State Ionic Devices*, World Scientific, Singapore (1988).
2. K. Kanehori, K. Matsumo, K. Miyauchi, and T. Kudo, *Solid State Ionics*, **9,10**, 1445 (1983).
3. S. D. Jones, J. R. Akridge, and F. K. Shokoohi, *Solid State Ionics*, **69**, 357 (1994).
4. C. Julien and G. A. Nazri, *Solid State Batteries: Materials Design and Optimization*, p. 579, Kluwer, Boston (1994).
5. J. B. Bates, N. J. Dudney, G. R. Gruzalski, R. A. Zuhr, A. Choudhury, C. F. Luck, and J. D. Robertson, *J. Power Sources*, **43/44**, 103 (1993).
6. J. B. Bates, G. R. Gruzalski, N. J. Dudney, C. F. Luck, and X. Yu, *Solid State Ionics*, **70/71**, 619 (1994).
7. N. J. Dudney, J. B. Bates, R. A. Zuhr, J. D. Robertson, H. P. Jun, and S. A. Hackney, *J. Electrochem. Soc.*, **146**, 2455 (1999).
8. Y. Shao-Horn, S. A. Hackney, A. R. Armstrong, P. G. Bruce, and R. Gitzendanner, *J. Electrochem. Soc.*, **146**, 2404 (1999).
9. M. Giorgetti, S. Passerini, W. H. Smyrl, S. Mukerjee, X. Q. Yang, and J. McBreen, *J. Electrochem. Soc.*, **146**, 2387 (1999).
10. L. Hernan, J. Morales, L. Sanchez, and J. Santos, *Solid State Ionics*, **118**, 179 (1999).
11. J. Kawakita, M. Takashi, and T. Kishi, *Solid State Ionics*, **120**, 109 (1999).
12. S. G. Kang, S. Y. Kang, K. S. Ryu, and S. H. Chang, *Solid State Ionics*, **120**, 155 (1999).
13. A. C. Hillier, S. Kim, and A. J. Bard, *J. Phys. Chem.*, **100**, 18808 (1996).
14. S. D. Alekperov, S. I. Vasil'ev, A. A. Kononenko, E. P. Lukashev, V. I. Panov, and A. E. Semenov, *Sov. Phys. Dokl.*, **33**, 828 (1988).
15. S. D. Alekperov, S. I. Vasiljev, A. A. Kononenko, E. P. Lukashev, V. I. Panov, and A. E. Semenov, *Chem. Phys. Lett.*, **164**, 151 (1989).
16. A. Semenov, J. P. Spatz, M. Möller, J.-M. Lehn, B. Sell, D. Schubert, Ch. H. Weidl, and U. S. Schubert, *Angewandte Chemie Intern. Ed. Engl.*, **38**, 2547 (1999).
17. A. Semenov, J. P. Spatz, J.-M. Lehn, Ch. H. Weidl, U. S. Schubert, and M. Möller, *Appl. Surf. Sci.*, **144-145**, 456 (1999).
18. M. Garcia, E. Webb, and S. H. Garofalini, *J. Electrochem. Soc.*, **145**, 2155 (1998).
19. M. Garcia and S. H. Garofalini, *J. Electrochem. Soc.*, **146**, 840 (1999).
20. D. A. Hensley and S. H. Garofalini, *J. Electrochem. Soc.*, **145**, 669 (1998).
21. R. L. Smith, W. Lu, and G. S. Rohrer, *Surf. Sci.*, **322**, 293 (1995).
22. G. Deo and I. E. Wachs, *J. Phys. Chem.*, **95**, 5889 (1991).
23. V. S. Pankajakshan, K. Neelakandan, and C. S. Menon, *Thin Solid Films*, **215**, 196 (1992).
24. J. B. Bates, N. J. Dudney, B. J. Neudecker, F. X. Hart, H. P. Jun, and S. A. Hackney, *J. Electrochem. Soc.*, **147**, 59 (2000).
25. J.-S. Bae and S.-I. Pyun, *J. Alloys Compd.*, **217**, 52 (1995).
26. R. Young, J. Ward, and F. Scire, *Rev. Sci. Instrum.*, **43**, 999 (1972).